

Effect of satellite based rainfall products on river basin responses of runoff simulation on flood event

Kwanchai Pakoksung¹ · Masataka Takagi¹

Received: 14 July 2016 / Accepted: 15 July 2016 / Published online: 29 July 2016
© Springer International Publishing Switzerland 2016

Abstract Physically-based distributed hydrological modelling, Rainfall-Runoff-Inundation (RRI) model is used to evaluate runoff accuracy by using six satellite based rainfall products such as GPM, GSMaP, TRMM 3B42V7, CMORPH, and PERSIANN. These products input to drive the model on the Nan River basin, Thailand that is the watershed of 13,000 km². The performance of the precipitation products, rainfall depth and runoff, was evaluated from storm event on 2014 by using statistical approach, Volume bias, Peak bias, RMSE, Correlation, and Mean bias, to compare with observation data. Overall of the satellite based products, the CMORPH and GPM performed the best that was provided by the statistical values, comparing with average observed rainfall data. For the runoff estimated from GPM closed to the observed data and was better than other five products, satellite and rain gauge, to provide the high correlation and small RMSE value. This study presents the uncertainty of satellites that have a potential for runoff estimation to apply for water resources management.

Keywords Rainfall spatial · Satellite based rainfall · Runoff · Rainfall-Runoff-Inundation model

Introduction

Rainfall is a definition to be the main component to estimate runoff based on the hydrological mechanism. Consequently, the spatial of rainfall is directly impacts

the hydrological system on a distributed hydrological model, several researches have focused on the outcome on discharge. Goodrich et al. (1995) reported that uniform rainfall can be applied for modelling the runoff on small catchments although the rainfall spatial has significant impact to discharge. Schuurmans and Bierkens (2007) point out a single rain gauge has carried a false prediction if it located outside the watersheds, and rainfall spatial is essentially for runoff modelling. Their conclusion is summarized by using the eight rainfall scenario based on spatial either distribution or uniform resulting from the distributed hydrological model of small catchment. Tsintikidis et al. (2002) and Chintalapudi et al. (2012) noted that watersheds contain with the sparse distribution of rain gauges, it cannot capture a spatial of rainfall for runoff modelling. Rainfall variable is direct to essential discharge for frequent events proposed by Arnaud et al. (2002). This study is done by using four artificial catchments of 20–1500 km² and three different hydrological models. Bell and Moore (2000) present an implementation of high spatial resolution of rainfall that has specially utilized in the convective rainfall event case.

A promising approach to capture the rainfall spatial is satellite based data. Near real time satellite products are now conveniently obtainable in the world, especially in developing countries. The uses of earth observation satellites have been about 30 years ago however these data have contained error from estimating rainfall dataset. In a recent year, the rainfalls produced by satellite have been increasing to application on basin scale of distributed hydrological model. Accuracy of satellite rainfall data have been increased as GPM data that is the new open source satellite product generated by using several new techniques such as merge different satellite.

✉ Kwanchai Pakoksung
178011e@gs.kochi-tech.ac.jp

¹ Kochi university of technology, Kami, Japan

Modelling of hydrological processes to generate runoff have used a several different satellite based rainfall products, Global Satellite Mapping of Precipitation (GSMaP), Tropical Rainfall Measuring Mission (TRMM), CPC MOPGHing technique (CMORPH), and Precipitation Estimation from Remotely Sensed Information using Artificial Neural Networks (PERSIANN). Sayama et al. (2012) demonstrated that GSMaP data performed a good agreement simulated by using the Rainfall-Runoff-Inundation model for large-scale area flood, in comparing its discharge and inundation results with observed data and referent flood map produced by MODIS satellite. Pakok-sung and Takagi (2015) showed that TRMM precipitation data performed the better precipitation data set to simulate runoff in the upper part of Nan river basin, Thailand, whereas Tan et al. (2015) showed that TRMM estimated a good rainfall rates that CMORPH and PERSIANN rainfall product over Malaysia. Jiang et al. (2010) used CMORPH product to simulate runoff that the result were better correlation than TRMM, to implement in the Laohahe river basin, northern part China. Chintalapudi et al. (2014) recommended that PERSIANN represented by coarse resolution data have produced better discharge results than higher resolution data such as TRMM over the Guadalupe watershed in USA.

The main objective of this research is to consider how well satellite rainfall products can capture the rainfall in temporal and spatial for purposing on rainfall-runoff modelling. The study area is located in the northern of the Thailand represented by a rural catchment of 13,000 km². RRI model based on a physical based rainfall-runoff modelling is available from modelling runoff for this study area. For this study area, satellite based rainfall as well as data from a rain gauge are available. Rainfalls were interpolated by the rain gauge as well as the satellite based rainfall products that are used to define the rainfall spatial during the wet season 2014. The rainfall characteristic in spatial and temporal is anticipated for the river basin catchment scale, especially at small time series even such as flood even. The different rainfall datasets are utilized in a sensitivity study such as input to the RRI model, and its results are compared with observation discharge hydrograph. The sensibility of the river basin scale response computed by using the model is hypothesized to reflect the actual river basin scale response. This study was achieved only for a sensitivity study, while its calibration was not performed. The outcome from the RRI model on runoff was investigated only the impact of different precipitation input, whereas the model calibration would mark the bias among input on the RRI variable.

The information of the river basin, data sets and the RRI model are described in Sect. 2 that is provided by the detail of rainfall data in the study area. Section 3 presents the

methodology such as storm event selection of rainfall, RRI model parameter setup, and performance statistic index. The results are shown in Sect. 4 with discharge hydrograph, while conclusions and discussion of the study are report in Sect. 5.

Data and hydrological modelling

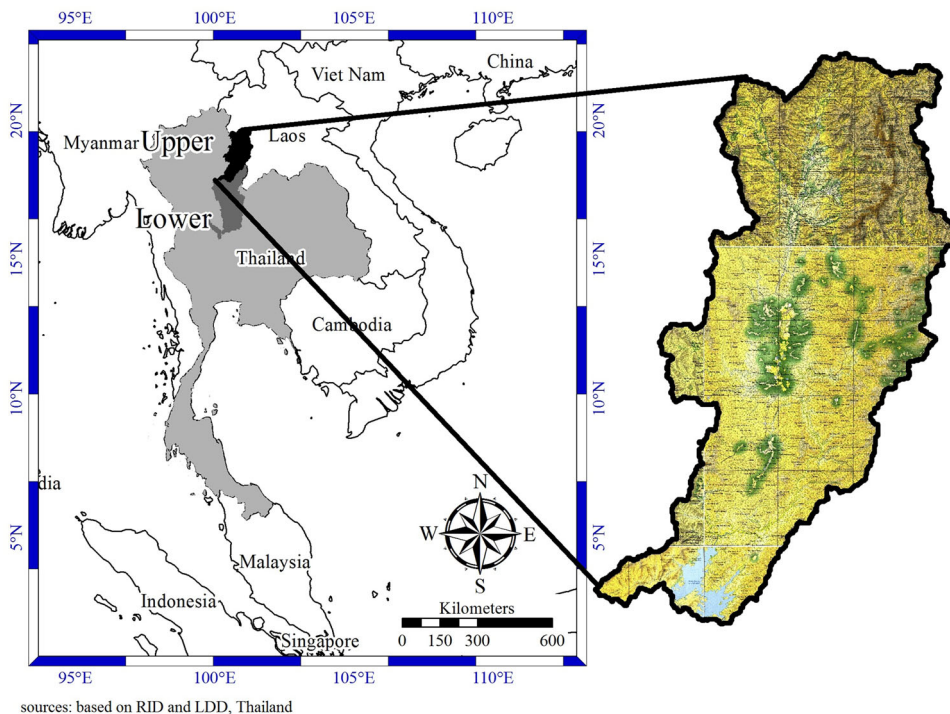
Study area

Nan River Basin in upper part area or upstream watershed of the SIRIKIT dam is important area because releases water of the SIRIKIT dam have been supplied for the central plain of Thailand, including Bangkok area. Figure 1 show the study basin area locates in the northern region of Thailand with the total catchment area of 13,000 km². The river originates from Bor Klua District, Nan Province, is situated between latitude 17°42'12"N to latitude 19°37'48"N and longitude 100°06'30"E to longitude 101°21'48"E. In this river basin, the mountain area accounts for 88 % and about 12 % residents inhabit in the middle of watershed. From the Sirikit dam identified as a river outlet of model to the upstream 150 km, the river bed slop is steep about 1/1500. Upstream of this part, the slop is flat (1/10,000) and next is very steep (1/600). The topography levels mention to mean sea level varies from 70 to 1200 m. The mean annual rainfall is 1380 mm. There are some important tributary such as the Wa River, Nam Pua River and Nam Yao River. Flooding in this area, over flow from river bank have occurred in some vulnerable area, Tawang Pha, Muang Nan and Wiang Sa district.

Topography data

Shuttle Radar Topography Mission (SRTM) provided by US Geological Survey (USGS) that was occurred from a joint mission between the National Imagery and Mapping Agency (NIMA) and the National Aeronautics and Space Administration (NASA). SRTM are available online on the Consultative Group for International Agriculture Research Consortium for Spatial Information (CGIAR-CSI). The SRTM data have covered the terrain of the Earth about 80 %, covering latitude 60° north to 56° south. This data as a digital elevation model (DEM) is based on 1 arc second or about 30 m not convenient for all countries but the 3 arc second (about 90 m) provided for the other location around the Earth. For the provided DEM, a vertical accuracy is 16 m to present in a linear error at 90 % confidence and a horizontal accuracy is 20 m to consider with circular error at 90 % confidence (Jarvis et al. 2012). According to the spatially pixel of SRTM DEM is about 90 m, but in this study it has been up scaled to 500 m of pixel size (about

Fig. 1 Location of the study area



15 × 15 arc-second). For numbers of pixel, row and column numbers are 457 and 292 respectively to present the watershed area (Fig. 3a) as 13,000 km². The index No. srtm_57_09 was downloaded above the study area.

Land cover and soil type

The land cover and soil type data sets were collected from Global Land Cover Characteristics (GLCC) of USGS and Land Development Department (LDD) of Thailand. These datasets were modified on a projection and down scaling to overlay to the DEM resolution. GLCC observed in 2000 is 1 km resolution from Advanced Very High Resolution Radiometer (AVHRR) in 10-day NDVI (Normalized Difference Vegetation Index) composites. These are core data set to use in a land cover characterization, during 1 year, April 1992 through March 1993 for source imagery data sets (Thenkabali et al. 2009). The land cover based on the GLCC data is shown in Fig. 3c that was divided by six types. Forest is dominant land cover on the study area with 70.69 % that are distributed over the border area of the watershed. Second largest land cover is crop-land about 14.58 %, followed as grassland (9.61 %), water bodies (2.1 %), deforestation (1.91 %), and urban area (1.1 %) (see Table 1). The crop-land and urban area are along the main stream distributed in the flood plain area between upstream to middle part of the river basin. The soil type’s datasets provided from the LDD, Thailand in Fig. 3d were divided into nine types, of which stone type is located in

Table 1 Land cover classification in watershed presented on percentages

Land cover type	Percentage area (%)
Forest	70.69
Deforestation	1.91
Grasslands	9.61
Cropland	14.58
Urban and build-up	1.10
Water bodies	2.10

the mountain area and eight are located in the flood plain area. The stone area is the main soil type about 83.68 %, to follow with silty clay, clay loam, sand clay, sandy loam, silty loam, sand clay loam, loam, and clay (see Table 2).

Precipitation data

The ground rainfall observation product was collected from the Royal Irrigation Department (RID), Thailand. There are 28 stations as presented in Fig. 3b, of which 17 stations are located in the study area while 11 stations are located on the west side. The rain gauge temporal data is daily datasets during 28 years (1988–2015). The 28 stations were used to construct the rainfall spatial distribution by using Kriging algorithms. The semi-variogram model of the Kriging method is based on the spherical semi-variogram equation, that the geostatistical theoretical can be referred

Table 2 Soil textural classification in watershed presented on percentages

Soil textural	Percentage area (%)
Clay	0.07
Clay loam	2.29
Loam	0.14
Sand clay	1.29
Sand clay loam	0.28
Sandy loam	1.00
Silty clay	10.74
Silty loam	0.52
Stone	83.68

to the previous studies (Chiles and Delfiner 1999; Webster and Oliver, 2007; Ly et al. 2011). Model parameter, the nugget variance (C_0) is 0.425, the partial sill (C) is 1.404 and the range (a) is 0.545° , are analysed from the observed rain gauges and applied for interpolating to grid spatial rainfall to represent the observed rainfall.

Global Precipitation Measurement (GPM) mission is originated generally from the United States and Japan that have been supported from Europe, France, India, and China with international cooperation. In this development, the microwave radiometers have investigated a microwave emission from precipitation is measured on many low-orbit satellites and downscaled into the interval to 3 h in exploration time for each area on the earth (Kubota et al. 2014). However, the sampling error problem occurs when the global precipitation data are smaller than 3 h. Therefore, it is essential for implementing a gap-filling algorithm for creating precipitation maps with high definition on temporal scale, which is moderately significant to apply such as flash flood warning systems.

The Global Satellite Mapping of Precipitation (GSMaP) development is supported and developed by JST-CREST and the JAXA Precipitation Measuring Mission (PMM) Science Team respectively (Okamoto et al. 2005). GSMaP, have applied the Kalman filter algorithm to estimate the current surface rainfall intensity from the infrared brightness temperature about 0.1° pixel size, using the GEO-IR satellites, is implemented for this study. The detail of the algorithm can be referred in the literature (Aonashi and Liu, 2000; Ushio et al. 2009). The GSMaP contained by the highest temporal and spatial resolution, can capture a precipitation event with real situation as observed rainfall, however, the precipitation quantity mostly has been underestimated (Fukami et al. 2010; Kubota et al. 2009; Makino, 2012; Seto 2009; Shretha et al. 2011). The GSMaP presents a good correlation on monthly and daily data using data in Japan (Seto 2009), which appear to be enough for flood early warning.

Tropical Rainfall Measuring Mission (TRMM) on 3B42V7 collected product number is the satellite based rainfall that locates in the tropical zone in the present day, which is a joint operation between NASA of USA and JAXA of Japan under the cooperation project in monitoring and exploration of space (Huffman et al. 2007). TRMM is the first satellite for monitoring variables, dynamic of precipitation, and latent heat of the precipitation process. The precipitation in the tropical zone is two-third of the total precipitation in the world, which plays an important role of the weather cycle. TRMM measurement is the combination between visible infra-red and microwave sensor with high frequency for monitoring and recording data both space and time. The satellite operation has been built for measuring the occurrence of precipitation both in the earth and the equatorial since 1997. The satellite is consisted by five main type sensor, Precipitation Radar (PR), TRMM microwave Image (TMI), Visible Infra-red Scanner (VIRS), Clouds and the Earth's Radiant Energy System (CERES), and Lighting Imaging Sensor (LIS). It has a circular and non-sun-synchronous orbit. The satellite observes from 305 km above the ground and 35° of orbit angle to equator, and it moves around the earth in 90 min or 16 times a day.

CPC Morphing Technique (CMORPH) presents a global precipitation data in real-time monitoring for global scale and has established by NOAA's Climate Prediction Center (CPC). CMORPH has provided the high resolution about 8 km spatial and 30 min temporal scale. In the CMORPH technique, the sensors, geostationary satellite IR temperature data and polar orbiting passive microwave (PMW), are implemented. The morphing algorithm is used to estimate the precipitation by the PMW and interpolate temporal weight in linearly (Joyce et al. 2004). In this study, the CMORPH resolution about 0.25° spatial and 3 h temporal product is implemented for comparing with other satellite rainfall; this product can be download from National Centers for Environmental Prediction (NCEP) CMORPH website.

Precipitation Estimation from Remotely Sensed Information using Artificial Neural Networks (PERSIANN) is developed by using the artificial neural networks (ANN) for monitoring rainfall intensity based on merged infra-red product of brightness temperature from geostationary satellite (Hong et al. 2004). The detailed procedure of developing PERSIANN products are explained in the study of Sorooshian et al. (2014). This study implemented to use the PERSIANN about 0.25° spatial and 3 h temporal resolution products to compare with the other satellite products, that the dataset can be downloaded from the PERSIANN website.

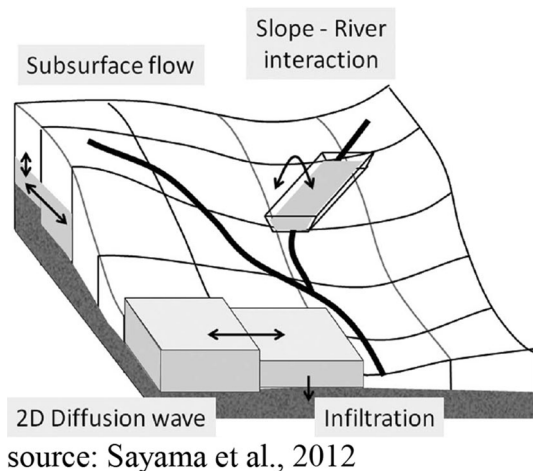


Fig. 2 RRI model schematic

Rainfall-Runoff-Inundation (RRI) model

Rainfall-runoff-inundation (RRI) model, a new developed model in a two dimension, was established by Dr. Sayama on 2010. Figure 2 is shown the model to deal with slopes and river channels. The river channel is located on the grid cell while the model assumes both slope and river as the same grid cell. The channel is assumed as a single direction along the centreline of the slope grid cell. This channel denotes an extra flow path between grid cells lying over the actual river course. Lateral flows are simulated on slope cells on a two dimensional basis. Slope grid cells on the river channel include two water depths, the channel and the slope (or floodplain). Inflow-outflow interacted between the slope and river is computed based on different overflowing formulae to depend on conditions of water-level and levee-height. Flow rate equation in governing equation of the RRI model is mass balance equation based on continuity equation as Eq. (1). For unsteady flow, the momentum equation is included in the governing equation of the RRI model in *x* Eq. (2) and *y* Eq. (3) directions.

$$\frac{\partial h}{\partial t} + \frac{\delta q_x}{\delta x} + \frac{\partial q_y}{\partial y} = r, \tag{1}$$

$$\frac{\partial q_x}{\partial t} + \frac{\partial u q_x}{\partial x} + \frac{\partial v q_x}{\partial y} = -gh \frac{\partial H}{\partial x} - \frac{\tau_x}{\rho_w}, \tag{2}$$

$$\frac{\partial q_y}{\partial t} + \frac{\partial u q_y}{\partial x} + \frac{\partial v q_y}{\partial y} = -gh \frac{\partial H}{\partial y} - \frac{\tau_y}{\rho_w}, \tag{3}$$

where *h* is the water height in local surface, *t* is the time step, *q_x* and *q_y* are discharge per unit width in *x* and *y* directions, *r* is rainfall intensity or lateral inflow, *H* is the height of water from a datum, *u* and *v* are flow velocities in *x* and *y* directions, *ρ_w* is the density of water, *g* is gravitational acceleration, and *τ_x* and *τ_y* are shear stress in *x* and

y directions. On the right hand side of Eqs. (1) and (2), a second term is computed by using Manning’s equation. The RRI model is used to apply diffusive wave routing for solving the two-dimensional equation by using the fifth-order Runge–Kutta method in numerical scheme. In Fig. 2, water surface slope is estimated by using difference of water height from cell 1 to cell 2 based on combination between water depth and ground elevation.

Methodology

The uncertainty of five satellite based rainfall products were investigated in this study, of which two are high resolution dataset and three are low resolution dataset. The accuracy of the satellite data product was assessed at daily time scale by comparing with the rain gauges. Using the five products as input to the RRI model, their outputs have performed an accuracy assessment with observation discharge at runoff station (Fig. 3b) on the five performance statistical coefficients.

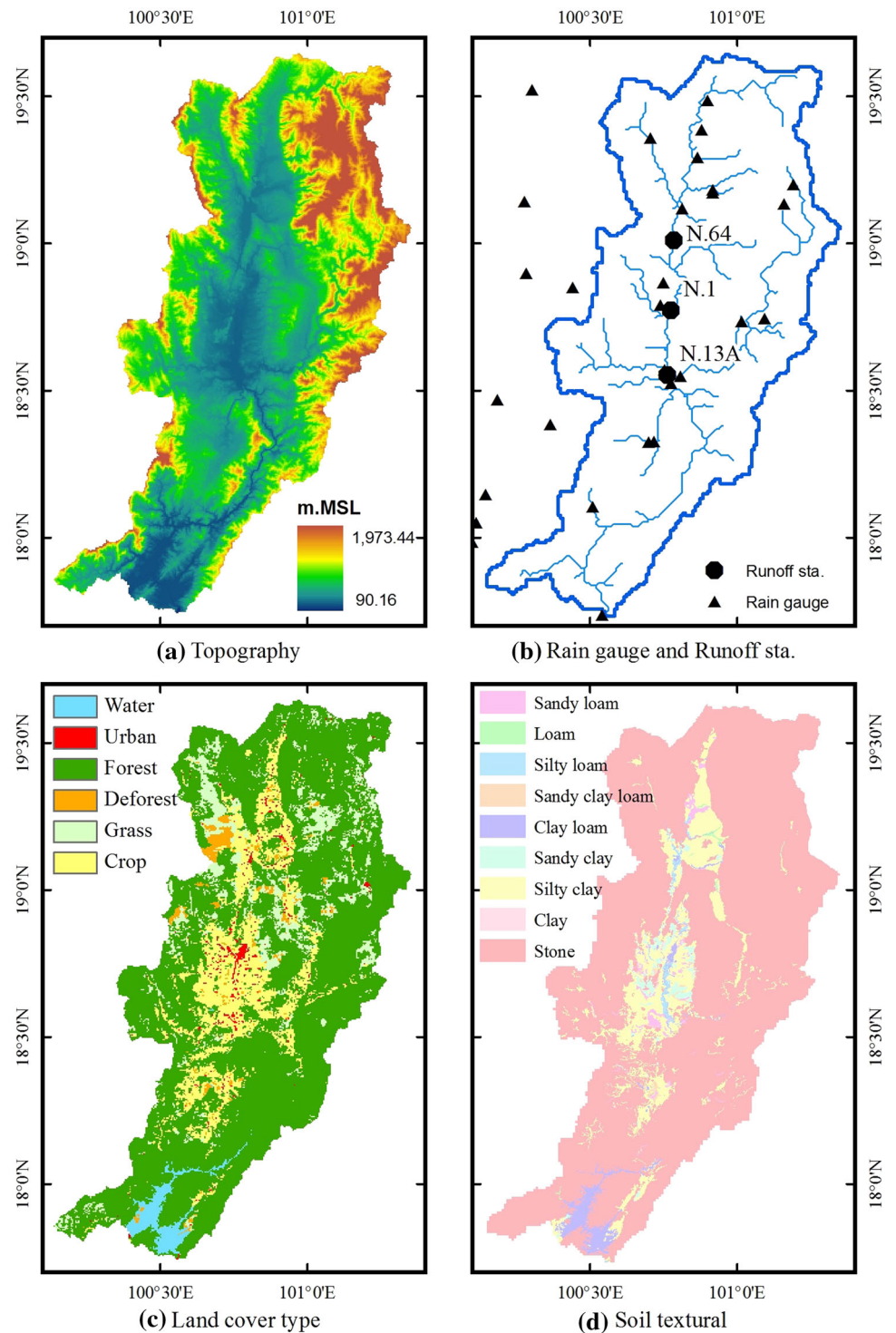
Storm event selection

The availability of different satellite products is presented in the Table 3 with GPM only available from April 2014 and TRMM to June 2015. Hence, the simulated storm event is selected from April 2014 to June 2015. According to the objective of this study is specific to the flood event that the storm event on the selected period occurs in the study area from monsoon during August to September. Large monsoon during 28–30 August 2014 across the northern part of Thailand brought a heavy rainfall about 100–150 mm. The heavy rainfall caused severe flooding and river bank over flow. Thus, the five satellite-based rainfall products were collected from August, 15 to September, 14 covering the flood event of the study area (Fig. 4).

Simulation model set-up

Input data sets of the RRI model are four data types; rainfall product, DEM presenting the topography from SRTM such as 500 m resolution, land cover using GLCC and soil type. On the definition of the distributed hydrological model to implement on the RRI model, the used hydrological parameters in this study are recommended by previous study such as Chow et al. (1988); Sayama et al. (2012); Sriariyawat et al. (2013); Pakoksung and Takagi (2015). Those parameters have been based on calibration in previous RRI model studies. According to the mathematics modelling of the RRI model, flow routing is based on the Manning’s roughness that correlates

Fig. 3 Watershed datasets in the study area



source: RID and LDD, Thailand

with the land cover type. Table 4 show the Manning’s roughness of the land covers type in this study. According to the hydrological soil type parameters represented by the Green-Amp parameter of soil is presented in Table 5. The parameters as shown in the Tables 4 and 5 were

utilized to simulate on the RRI model for different rainfall sources.

For the characteristic of river channel, the re-sampled DEM was used for generating a flow direction to identify with eight directions, 0°, 45°, 90°, 135°, 180°, 225°, 270°

Table 3 Information of rainfall products

No.	Name	Spatial/temporal resolution	Covering	Period	References
1	Rain gauges	Point data	Study area	1987-present	RID, Thailand
2	GPM	0.10°/0.5 h	Global/(90°N–S)	2014-present	Kubota et al. (2014)
3	GSMaP	0.10°/0.1 h	Global/(60°N–S)	2006-present	Okamoto et al. (2005)
4	TRMM	0.25°/3.0 h	Global/(50°N–S)	2000-Jun, 2015	Huffman et al. (2007)
5	CMORPH	0.25°/3.0 h	Global/(50°N–S)	2002-present	Joyce et al. (2004)
6	PERSIANN	0.25°/3.0 h	Global/(60°N–S)	2000-present	Sorooshian et al. (2014)

Fig. 4 Average satellite based rainfall product over the study area in temporal scale

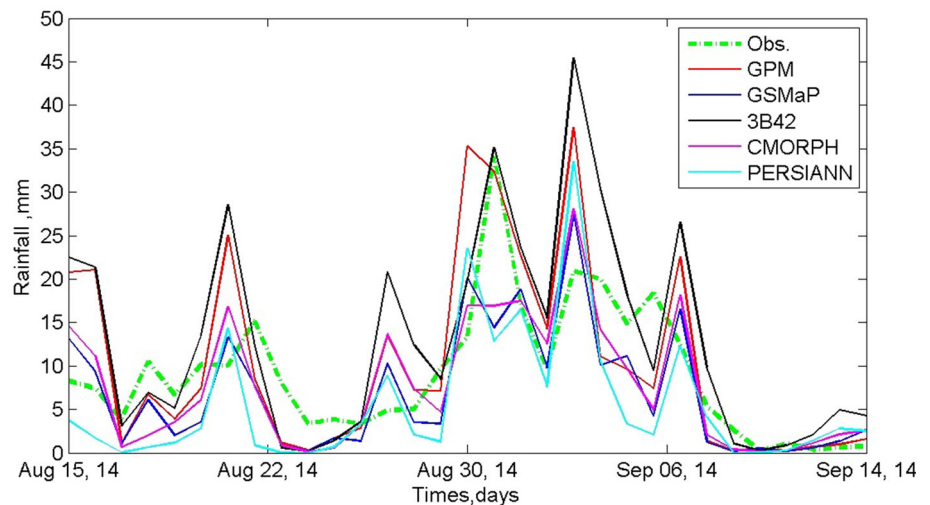


Table 4 Land cover parameter represented by the n manning coefficient

Land cover type	n manning
Forest	0.50
Deforestation	0.40
Grasslands	0.30
Cropland	0.35
Urban and build-up	0.05
Water bodies	0.04

and 315°, depended on elevation of downstream pixel. The flow direction was used for counting numbers of the upstream pixels to identify a flow accumulate value to a specific pixel. In this study, the flow accumulation was used for estimation width and depth of the river channel followed as Eqs. (4) and (5) by Sayama et al. 2012.

$$W = 16.93 \cdot A_{basin}^{0.186}, \tag{4}$$

$$D = 16.93 \cdot A_{basin}^{0.120}, \tag{5}$$

where W is the channel width in m, A_{basin} is the catchment area in km^2 , and D is the channel depth in m.

Performance statistical

The estimation results driven by the several spatial distribution methods based on the daily rain gauge data were evaluated to analysis bias of runoff volume (V_{bias}), bias of peak discharge (P_{bias}), root mean square error ($RMSE$), correlation coefficient (R^2), and mean error (ME). The following formulas (see Table 6) were applied to evaluate simulation performance. The volume bias and peak bias estimate the systematic bias of modelled runoff in percentage (%). The correlation index is quantification in correlation of two data sets, simulated and observed runoff, which 0 is no correlation while 1 is perfect correlation. The $RMSE$ is a different measure of difference magnitude between two datasets, while the ME is the bias from two datasets.

Results and discussion

Rainfall products

All rainfall products of satellite were implemented with different resolution of spatial and temporal. GPM and GSMaP have the high resolution of spatial scale about 0.1°

Table 5 Soil type parameter represented by the Green-Ampt coefficient

Soil textural	Soil depth (m)	Saturated hydraulic conductivity (ka), (cm/h)	Green-Ampt parameter		
			K (cm/h)	Porosity	Capillary head (cm)
Clay	1.0	0.462	0.06	0.475	31.63
Clay loam	1.0	0.882	0.20	0.464	20.88
Loam	1.0	2.500	1.32	0.463	8.89
Sandy clay	2.0	0.781	0.12	0.430	23.90
Sandy clay loam	1.5	2.272	0.30	0.398	21.85
Sandy loam	1.5	12.443	2.18	0.453	11.01
Silty clay	1.0	0.366	0.10	0.430	29.22
Silty loam	1.0	2.591	0.68	0.501	16.68
Stone	1.5	–	–	–	–

Table 6 Description of performance statistical

Statistical index	Description
Volume bias (%)	$V_{bias} = \frac{ Q_{vo} - Q_{vs} }{Q_{vo}} \times 100$
Peak bias (%)	$P_{bias} = \frac{ Q_{po} - Q_{ps} }{Q_{po}} \times 100$
Root mean square	$RMSE = \sqrt{\frac{\sum_{i=1}^n (Q_{o(i)} - Q_{s(i)})^2}{n}}$
Correlation	$R^2 = \frac{(\sum_{i=1}^n (Q_{o(i)} - \bar{Q}_o) \cdot (Q_{s(i)} - \bar{Q}_s))^2}{\sum_{i=1}^n (Q_{o(i)} - \bar{Q}_o)^2 \cdot \sum_{i=1}^n (Q_{s(i)} - \bar{Q}_s)^2}$
Mean bias	$ME = \frac{\sum_{i=1}^n (Q_{o(i)} - Q_{s(i)})}{n}$, where Q_{vo} is observation volume Q_{vs} is simulation volume Q_{po} is observation peak Q_{ps} is simulation peak Q_o is observation data Q_s is simulation data n is total number of sample

and different temporal scale of 0.5 and 1.0 h, respectively. TRMM 3B42V7, CMORPH, and PERSIANN have the course resolution about 0.25° of spatial and 3.0 h of temporal. Figure 4 show the watershed average rainfall comparison during the flood event on 2014 (August, 15 to September, 14). All satellite products were quite different from the observed rainfall pattern at some peak. On the first peak, all products were different from the observed data on magnitude and time. The TRMM showed highest overestimation, while GSMaP and PERSIANN revealed the similar magnitude. At the third peak, the TRMM and GPM presented the best fit on magnitude; however, the GPM was different on time scale about 1 day. The other three products were difference value at this peak. The fourth and fifth peak was quite different on overestimation.

Figure 5 shows the average spatial distribution of satellite-based rainfall and ground observation products during the storm event. During in the period 30 days, the differences rainfall values were about 1–18 mm over space of 200 km. The TRMM 3B42V7 rainfall products presented that maximum rainfall intensities were located in the

western part along the border of watershed and also the other three products (GSMaP, CMORPH, and PERSIANN). This distribution was similar to the observed spatial interpolation product, but it was different in the northern part. By the contract, the high intensities of GPM were in the northern part inside the boundary of the watershed, that the spatial pattern was similar to the observed rainfall spatial. However, the GPM was different in the western part.

The total rainfall amount for five satellite-based rainfall and ground observation products for flood events in 2014 were presented in the Table 7, which was estimated by accumulating the rainfall input over the catchment area. In overall, TRMM was the largest amount of rainfall volume followed by GPM, while PERSIANN was smallest. The GPM and CMORPH presented the total volume close to the rainfall volume of rain gauge. However, the GPM was overestimation and the CMORPH underestimation the observation rainfall.

Effect of spatial distribution among the observation rain gauges

All satellite-based rainfall products revealed low accuracies by significant differences among comparing with rain gauges based on the performance statistical (Table 8). GSMaP and PERSIANN underestimated rainfall based on Volume bias by about 23.6 and 38.3 %, respectively. Mean bias revealed that both products underestimated rainfall about 2.15 and 3.5 mm/day, respectively. The both products were also underestimation, reported by the previous studies (Kidd et al. 2012; Tian et al. 2008; Qin et al. 2014; Sohn et al. 2009; Asadullah et al. 2010). The fact that most satellite based rainfall data have been represented in underestimation might be due to the algorithm of estimation (Tian et al. 2008). The GSMaP underestimate rainfall represented by the mean bias in China about 0.53 mm/day and also in Columbia about 2.3 mm/day (Qin et al. 2014;

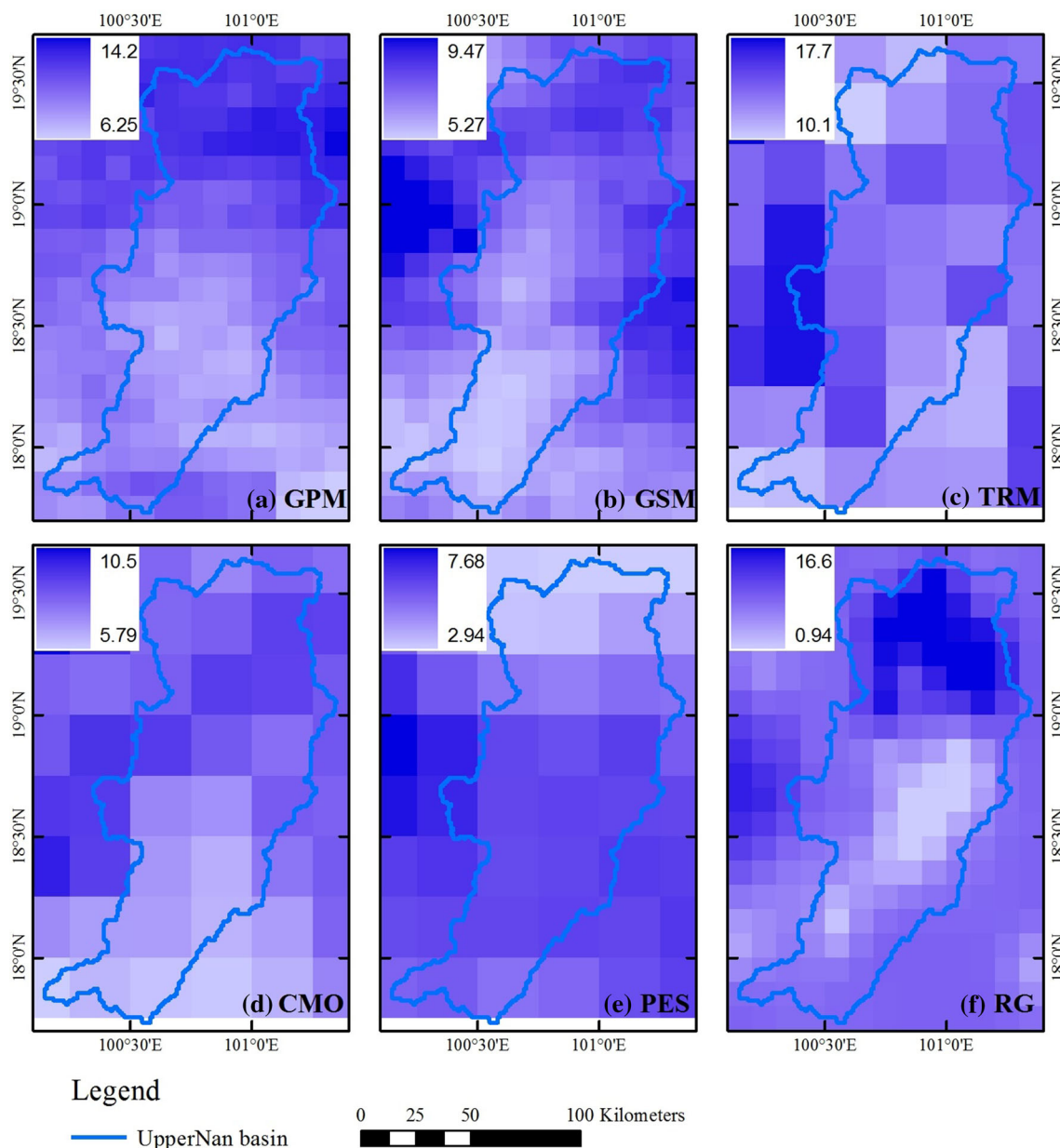


Fig. 5 Average satellite based rainfall spatial products

Dinku et al. 2010). TRMM and GPM represented by the Volume bias overestimated rainfall about 49.2 and 19.9 %, respectively. The Mean bias of both products was about 4.5 and 1.54 mm/day, respectively. Overestimation of TRMM has been reported by the previous studies that bias is about 30.5 % in the USA and 4.5 % in the China (Behrangi et al. 2011; Chen et al. 2011). It presented that the GPM has overestimated about 4.0 % in Iran (Sharifi et al. 2016). Volume bias and Mean bias of CMORPH on underestimation were 11.06 % and 1.01 mm/day, respectively. The CMORPH has underestimated rainfall reported by the other studies (Tan et al. 2015; Qin et al. 2014; Asadullah et al. 2010). This study found that the CMORPH was the best

performance compared with the other products.*The best evaluated value

The Underestimation of peak rainfall had occurred in four products, GPM, GSMaP, CMORPH, and PERSIANN, while TRMM overestimated peak rainfall. In overall, the TRMM performed the best match of peak bias, but the GPM was the best among the underestimation products. The low accuracies on comparison, GPM presented the best linear correlation with observed data ($R^2 = 0.327$) to follow with TRMM, GSMaP, CMORPH, and PERSIANN. All satellite products had range of RMSE about 16–20 mm/day. The GSMaP was the best performance with lowest RMSE value, and the TRMM was the highest value

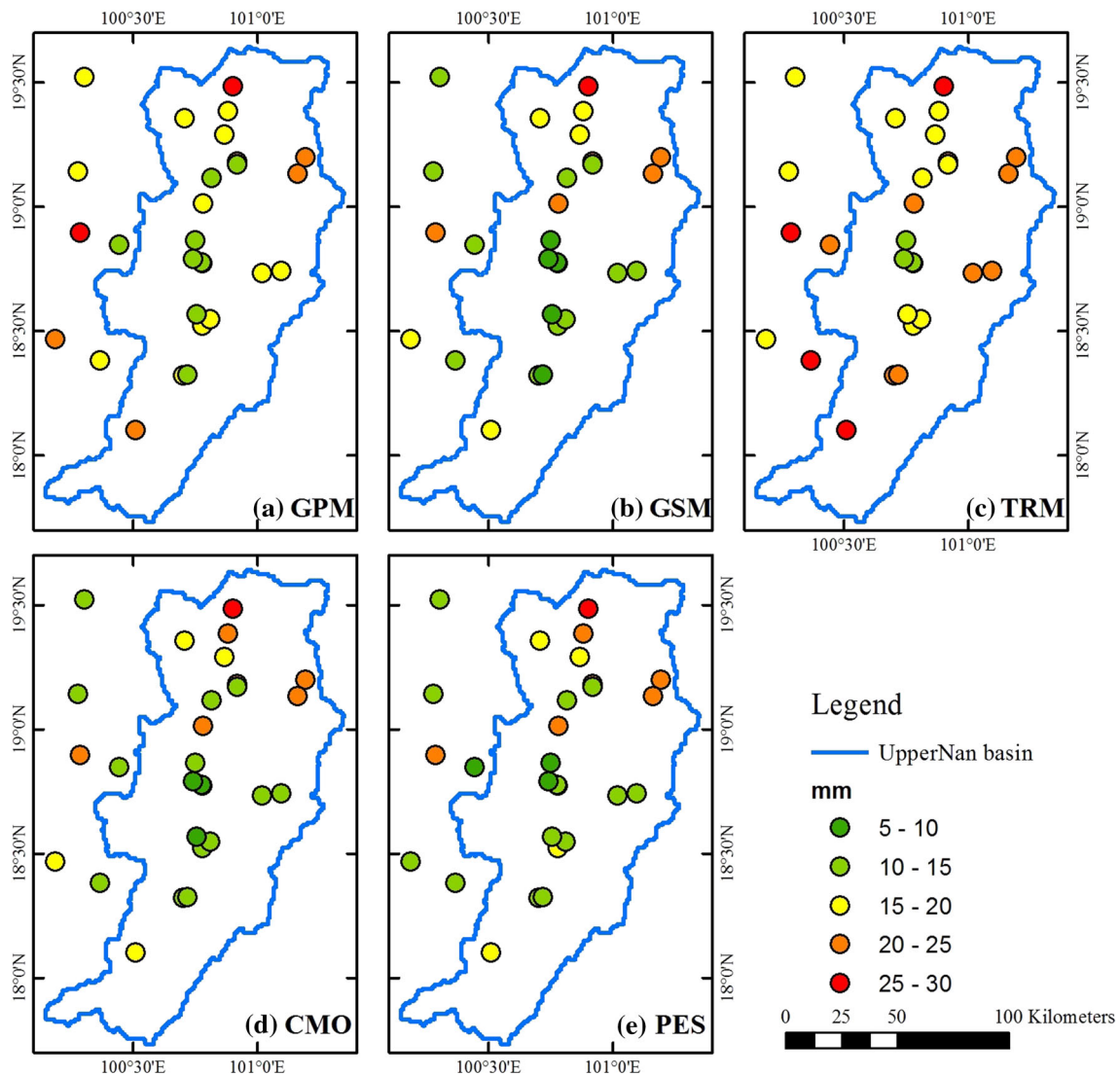


Fig. 6 Root mean square error (RMSE) daily rainfall between rain gauge and satellite based rainfall products

Table 7 Volume of rainfall products amounts over the study watershed

Rainfall products	Rainfall volume (MCM)
Rain gauge	7899.97
GPM	8495.00
GSMaP	5639.10
TRMM	12,254.51
CMORPH	7223.27
PERSIANN	5252.20

with low performance. The low performance of the TRMM based on the *RMSE* value could be referred by the previous study (Qin et al. 2014).

Estimation accuracy of evaluated satellite rainfall products over the Nan river basin of Thailand with information was based on the spatial distribution of *RMSE* from flood events in 2014. Figure 6 showed the *RMSE* of satellite-based rainfall products on the flood event, which GSMaP was the best agreement with the observed rainfall. Interestingly, the lowest *RMSE* value for all methods was found in the middle part of watershed boundary. The northern part and north-eastern part is represented by the high mountainous area, where all products have estimated on the high *RMSE* value. This indicated that the satellite-based rainfall could not explore to obtain a good performance covering the mountain area because of classification of warm clouds from the IR sensors and numerical modelling of microwave signal (Yilmaz et al. 2005; Huffman et al. 2007).

Table 8 Performance statistical of rainfall spatial products

Rainfall products	Volume bias (%)	Peak bias (%)	RMSE (mm)	Correlation	Mean bias (mm)
GPM	16.94	-5.33	18.15	0.327*	1.54
GSMaP	-23.66	-57.87	16.08*	0.270	-2.15
TRMM	49.21	2.89*	20.22	0.285	4.48
CMORPH	-11.06*	-50.44	16.46	0.258	-1.01*
PERSIANN	-38.35	-62.47	16.77	0.233	-3.49

* The best evaluated value

Runoff simulation

The hydrological model (RRI model) was driven for flood events in 2014. The six rainfall products was simulated at daily on a temporal scale to match the Royal Irrigation Department Thailand observed discharge data. Three observation stations were selected in the Nan river basin (Fig. 3b), the first one belonging to the upstream sub-catchment (N.64), the second one belonging to the middle area (N.1) and the third one belonging to the downstream area (N.13A), to show the daily hydrograph that results from the different interpolation scenario. Figure 7 present the hydrographs for all rainfall products with the three observation station, N64, N.1 and N.13A.

All simulated runoff driven by different products was to provide the temporal pattern similar to the observed hydrograph for the flood event. Over view of all the runoff station, GPM symmetrically captured the peak at the same time with the observation, while the other five products symmetrically lagged about 1 day. PERSIANN, GSMaP and CMORPH systematically underestimated observed runoff, while the other three products were underestimation. For N.13A, all patterns of rainfall products were underestimation to compare with the observed hydrograph.

All of three runoff station on the daily hydrograph were analysed and calculated for evaluation by the performance statistical. The results are given in Table 9 that is concluded by five indexes. GPM estimated discharge was the best closed to the observed data represented by the highest R^2 of 0.885 and lowest $RMSE$ of 141.77 m^3/s . This simulated runoff overestimated the runoff volume, peak flow and mean runoff by 10.6, 3.55 % and 44.6 m^3/s , respectively. TRMM simulated runoff was high Correlation and low $RMSE$, however, its simulated runoff was overestimation of Volume bias of 13.27 % and Mean bias of 55.84 %. The peak flow of the TRMM underestimated about 17.8 %. The three products, GSMaP, CMORPH and PERSIANN, was significantly underestimation on the runoff volume, mean runoff, and peak flow, with high $RMSE$ and low R^2 value. Rain gauge simulated runoff was low $RMSE$ value of 163.88 m^3/s with strong R^2 value of 0.821, this simulated results overestimated the runoff volume, and mean runoff by 6.4 %, 27 m^3/s , respectively. The peak flow of the Rain gauge underestimated about 34.6 %.

In summary performance on estimating the discharge, the best of the satellite-based rainfall products was GPM that statistical presented some value better than the Rain gauge interpolated product. The GPM product was represented on the high resolution products, while TRMM product was the best performance among the coarse resolution products.

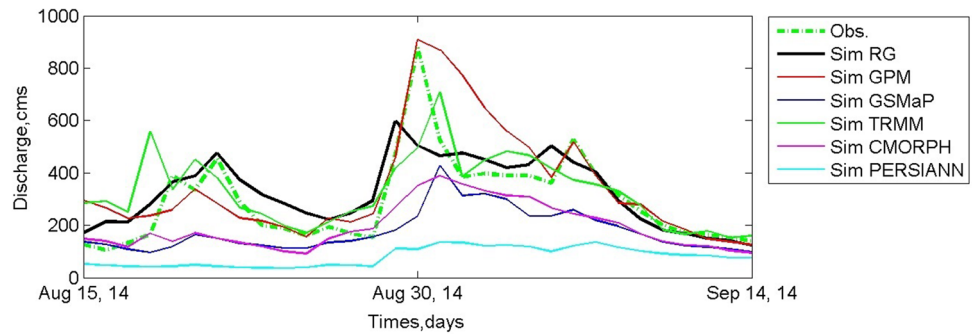
Conclusions

The evaluation of six rainfall products (Rain gauge, GPM, GSMaP, TRMM, CMORPH and PERSIANN) was input to the physical-based hydrological model (RRI model) over the Nan river basin Thailand. According to the aim of this study used the flood event for estimating the streamflow to evaluate the performance of each product. The simulation of the streamflow was done by using without a calibration of the hydrologic parameter to specific product. The streamflow were simulated and reported at daily to match with the RID observed runoff.

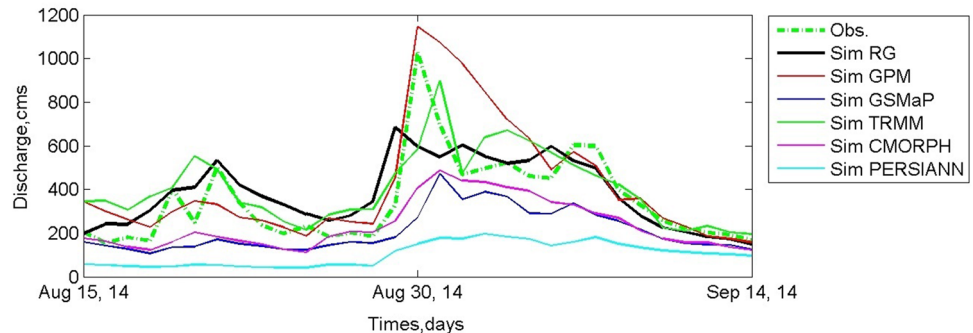
The average satellite-based rainfall product whole watershed a comparison results presented that the CMORPH, products were the best fit with volume and mean bias to the observed rainfall, however, there underestimation the peak flow. The results of well performance on the CMORPH agree with the previous studies (Dinku et al. 2008; Vera et al. 2012; Zeweldi et al. 2011). TRMM was overestimation the peak bias; however, it was the best performance of peak flow. GSMaP presented the lowest value of the $RMSE$ that indicated the best degree of estimates different from the observation. GPM indicated the best degree of the linear relationship between estimation and observation with the correlation measures.

GPM demonstrated to be the best satellite-based rainfall product to model a streamflow for flood event on 2014. The result of the GPM agrees with the previous study (Tang et al. 2016). The simulated runoff of TRMM also closed to the observed dataset; however, it overestimated the runoff volume and mean runoff. The peak flow of the TRMM was underestimation. GSMaP and CMORPH underestimation the runoff volumes, mean runoff, and peak flow. PERSIANN was the highest

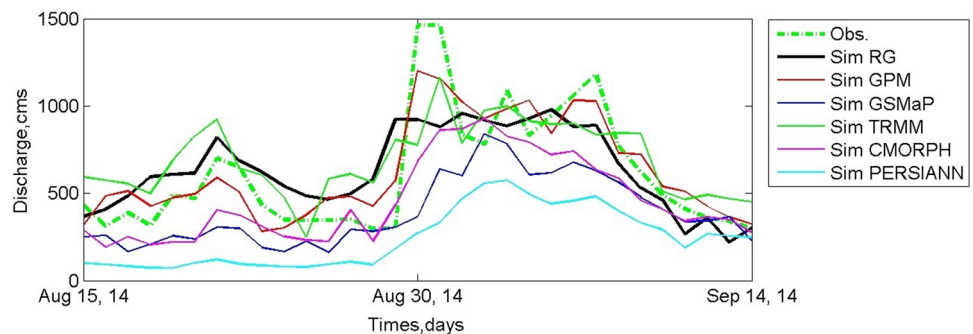
Fig. 7 Daily discharge hydrograph at runoff observation station of flood event based on satellite base rainfall products



(a) N.64



(b) N.1



(c) N.13A

Table 9 Performance statistical of runoff from the rainfall spatial prediction products

Rainfall products	Volume bias (%)	Peak bias (%)	RMSE (cms)	Correlation	Mean bias (cms)
Rain gauge	6.40*	-34.60	163.88	0.821	26.94*
GPM	10.60**	3.55*	141.77*	0.885*	44.61**
GSMaP	-39.05	-54.02	266.06	0.681	-164.39
TRMM	13.27	-17.86	192.35	0.761	55.84
CMORPH	-30.35	-48.51	222.88	0.767	-127.73
PERSIANN	-66.43	-73.86	348.26	0.742	-279.60

* The best evaluated value

** The best evaluated value among the satellite based rainfall data

underestimation of runoff volume, peak and mean runoff, with high RMSE and weak correlation value. In conclusion, the GPM simulated was the best performance satellite product for hydrological modelling to estimate the runoff on the river basin scale, representing with the

high resolution products. However, the TRMM was the best among the course resolution products.

Satellite-based rainfall products, can capture the overall rainfall pattern, are alternative for implementation in the remote area such as the ungauged basins. Among five

satellite-based rainfall products, GPM and TRMM have potential to produce a simulated streamflow on the hydrological modelling. The satellite-based rainfall products might be needed a bias correction before application as input to the hydrological modelling. More studies on the bias correction of satellite rainfall products are in the literatures (Habib et al. 2014; Muller and Thompson, 2013; Vernimmen et al. 2012).

Acknowledgments The study cannot be conducted without the data provided from various agencies. Kochi University of Technology has been supported in the part with Takagi laboratory. The researchers would like to gratefully thank to Dr. Takahiro Sayama, the Associate Professor of Disaster Prevention Research Institute at Kyoto University, for the RRI model.

References

- Aonashi K, Liu G (2000) Passive microwave precipitation retrievals using TMI during the Baiu period of 1999. Part I: algorithm description and validation. *J Appl Meteor.* 39:2024–2037
- Arnaud P, Bouvier C, Cisner L, Dominguez R (2002) Influence of rainfall spatial variability on flood prediction. *J Hydrol* 260:216–230
- Asadullah A, Mcintyre NEIL, Kigobe MAX (2010) Evaluation of five satellite products for estimation of rainfall over Uganda. *Hydrolog Sci J* 53:1137–1150
- Behrangi A, Khakbaz B, Jaw TC, AghaKouchak A, Hsu K, Sorooshian S (2011) Hydrologic evaluation of satellite precipitation products over a mid-size basin. *J Hydrol* 397:225–237
- Bell VA, Moore RJ (2000) The sensitivity of catchment runoff models to rainfall data at different spatial scales. *Hydrol Earth Syst Sci* 4:653–667
- Chen C, Yu Z, Li L, Yang C (2011) Adaptability evaluation of TRMM satellite rainfall and its application in the Dongjiang river basin. *Proced Environ Sci* 10:396–402
- Chiles JP, Delfiner P (1999) *Geostatistics: modelling spatial uncertainty*. John Wiley & Sons, New York
- Chintalapudi S, Sharif HO, Yeggina S, Elhassan A (2012) Physically-based, hydrologic model results based on three precipitation products. *J Am Water Resour Assoc JAWRA* 48:1191–1203
- Chintalapudi S, Sharif HO, Xie H (2014) Sensitivity of distribution hydrologic simulations to ground and satellite based rainfall products. *Water* 6:1221–1245. doi:10.3390/w6051221
- Chow VT, Maidment DR, Mays LW (1988) *Applied hydrology*, 6th edn. McGraw Hill International, New York
- Dinku T, Chidzambwa S, Ceccato P, Connor SJ, Ropelewski CF (2008) Validation of high-resolution satellite rainfall products over complex terrain. *Int J Remote Sens* 29:4097–4110
- Dinku T, Ruiz F, Connor SJ, Ceccato P (2010) Validation and intercomparison of satellite rainfall estimates over Colombia. *J Appl Meteorol Climatol* 49:1004–1014
- Fukami K, Shirashi Y, Inomata H, Ozawa G (2010) Development of integrated flood analysis system (IFAS) using satellite-based rainfall products with a self-correction method, International centre for water hazard and risk management under auspices of UNESCO (ICHARM). Public Works Research Institute, Tsukuba
- Goodrich DC, Faures JM, Woolhiser DA, Lane LJ, Sorooshain (1995) Measurements and analysis of small-scale convective storm rainfall variability. *J Hydrol* 173:283–308
- Habib E, Haile AT, Sazib N, Zhang Y, Rientjes T (2014) Effect of bias correction of satellite-rainfall estimates on runoff simulation as the source of the Upper Blue Nile. *Remote Sens* 6(7):6688–6708. doi:10.3390/rs6076688
- Hong Y, Hsu KL, Sorooshian S, Gao XG (2004) Precipitation estimation from remotely sensed imagery using an artificial neural network cloud classification system. *J Appl Meteorol* 43:1834–1852
- Huffman GJ, Adler RF, Bolvin DT, Gu GJ, Nelkin EJ, Bowman KP, Hong Y, Stocker EF, Wolff DB (2007) The TRMM multisatellite precipitation analysis (TMPA): quasi-global, multiyear, combined-sensor precipitation estimates at fine scales. *J Hydrometeorol* 8:38–55
- Jarvis A, Reuter HI, Nelson A, Guevara E (2012) Hole-filled SRTM for the Globe Version 4. CGIAR-CSI SRTM 90 m Database 2008, Available online <http://srtm.csi.cgiar.org>. Accessed 1 Jul 2012
- Jiang S, Ren L, Yong B, Yang X, Shi L (2010) Evaluation of high-resolution satellite precipitation products with surface rain gauge observations from Laohahe Basin in northern China. *Water Sci Eng* 3(4):405–417. doi:10.3882/j.issn.1674-2370.2010.04.004
- Joyce RL, Janowiak JE, Arkin PA, Xie P (2004) CMORPH: a method that produces global precipitation estimates from passive microwave and infrared data at high spatial and temporal resolution. *J Hydrometeorol* 5:487–503
- Kidd C, Bauer P, Turk J, Huffman GJ, Joyce R, Hsu KL, Braithwaite D (2012) Intercomparison of high-resolution precipitation products over northern Europe. *J Hydrometeorol* 13:67–83
- Kubota T, Ushio T, Shige S, Kida S, Kachi M, Okamoto K (2009) Verification of high resolution satellite-based rainfall estimates around Japan using a gauge calibrated ground radar data set. *J Meteorol Soc Jpn* 87A:203–222
- Kubota T, Seto S, Awaka J, Kida S, Oki R (2014) Evaluation of precipitation estimations by at-Launch codes of GPM/DPR algorithms using synthetic data from TRMM/PR observations. *IEEE J Sel Top Appl Earth Obs Remote Sens* 7(9):3931–3944. doi:10.1109/JSTARS.2014.2320960
- Ly S, Charles C, Degre A (2011) Geostatistical interpolation of daily rainfall at catchment scale: the use of several variogram models in the Ourthe and Ambleve catchments, Belgium. *Hydrol Earth Syst Sci* 15:2259–2274. doi:10.5194/hess-15-2259-2011
- Makino S (2012) Verification of the accuracy of rainfall data by global satellite mapping of precipitation (GSMaP) product, Yamaguchi University Thesis
- Muller MF, Thompson SE (2013) Bias adjustment of satellite rainfall data through stochastic modeling: methods development and application to Nepal. *Adv Water Resour* 60:121–134. doi:10.1016/j.advwatres.2013.08.004
- Okamoto K, Iguchi T, Takahashi N, Iwanami K, Ushio T (2005) The Global Satellite Mapping of Precipitation (GSMaP) project. In: 25th IGARSS Proceeding, pp 3414–3416
- Pakoksung K, Takagi M (2015) Remote sensing data application for flood modeling. *JAST* 26:115–122
- Qin Y, Chen Z, Shen Y, Zhang S, Shi R (2014) Evaluation of satellite rainfall estimates over the Chinese mainland. *Remote Sens* 6:11649–11672. doi:10.3390/rs61111649
- Sayama T, Ozawa G, Kawakami T, Nabesaka S, Fukami K (2012) Rainfall-runoff-inundation analysis of the 2010 Pakistan flood in the Kabul River basin. *Hydrol Sci J* 57:298–312. doi:10.1080/02626667.2011.644245
- Schuurmans JM, Bierkens MFP (2007) Effect of spatial distribution of daily rainfall on interior catchment response of a distributed hydrological model. *Hydrol Earth Syst Sci* 11:677–693. doi:10.5194/hess-11-677-2007

- Seto S (2009) An evaluation of overland rain rate estimates by the GSMaP and GPROF Algorithm: the role of lower frequency channels. *J Meteorol Soc Jpn* 87A:183–202
- Sharifi E, Steinacker R, Saghafian B (2016) Assessment of GPM-IMERG and other precipitation products against gauge data under different topographic and climatic conditions in Iran: preliminary results. *Remote Sens* 8(2):1–24
- Shretha V, Takara K, Kubota T, Bajracharya SR (2011) Verification of GSmaP rainfall estimates over the central Himalayas. *Hydraul Eng* 67(4):137–142
- Sohn BJ, Han HJ, Seo EK (2009) Validation of satellite-based high-resolution rainfall products over the Korean Peninsula using data from a dense rain gauge network. *J Appl Meteorol Climatol* 49:701–714
- Sorooshian S, Hau K, Braithwaite D, Ashouri H, NOAA CDR Program (2014) NOAA Climate Data Record (CDR) of Precipitation Estimation from Remotely Sensed Information using Artificial Neural Networks (PERSIANN-CDR), Version 1 Revision 1. NOAA National Climatic Data Centers for Environmental Information. doi:[10.7289/V51V5BWQ](https://doi.org/10.7289/V51V5BWQ)
- Sriariyawat A, Pakoksung K, Sayama T, Tanaka S, Koontanakulvong S (2013) Approach to estimate the flood damage in Sukhothai Province using flood simulation. *J Disaster Res* 8(3):406–414
- Tan ML, Ibrahim AL, Duan Z, Cracknell AP, Chaplot V (2015) Evaluation of six high-resolution satellite and ground-based precipitation products over malaysia. *Remote Sens* 7:1504–1528. doi:[10.3390/rs70201504](https://doi.org/10.3390/rs70201504)
- Tang G, Ma Y, Long D, Zhong L, Hong Y (2016) Evaluation of GPM Day-1 IMERG and TMPA Version-7 legacy products over Mainland China at multiple spatiotemporal scales. *J Hydrol* 533:152–167
- Thenkabali PS, Biradar CM, Noojipady P, Dheeravath V, Li Y, Velpuri M, Gumma M, Gangalakunta ORP, Turrall H, Cai X, Vithanage J, Schull MA, Dutta R (2009) Global irrigated area map (GIAM), derived from remote sensing, for the end of the last millennium. *Int J Remote Sens* 30:3679–3733. doi:[10.1080/01431160802698919](https://doi.org/10.1080/01431160802698919)
- Tian Y, Peters-Lidard CD, Adler RF, Kubota T, Ushio T (2008) Evaluation of GSMaP precipitation products. *Bull Am Meteorol Soc* 89:1911–1916
- Tsintikidis D, Georgakakos KP, Sperfsilage JA, Smith DE, Carpenter TM (2002) Precipitation uncertainty and rain gauge network design within Folsom Lake watershed. *J Hydrol Eng* 7:175–184
- Ushio T, Kubota T, Shige S, Okamoto K, Aonashi K, Inoue T, Takahashi N, Iguchi T, Kachi M, Oki R, Morimoto T, Kawasaki Z (2009) A Kalman filter approach to the Global Satellite Mapping of Precipitation (GSMaP) from combined passive microwave and infrared radiometric data. *J Meteorol Soc Japan* 87A:137–151
- Vera T, Rojas R, Zambrano-Bigiarini M, Levizzani V, de Roo A (2012) Validation of satellite-based precipitation products over sparsely gauged african river basins. *J Hydrometeorol* 13:1760–1783
- Vernimmen RRE, Hooijer A, Mamenun Aldrian E, van Dijk AIJM (2012) Evaluation and bias correction of satellite rainfall data for drought monitoring in Indonesia. *Hydrol Earth Syst Sci* 16:133–146. doi:[10.5194/hess-16-133-2012](https://doi.org/10.5194/hess-16-133-2012)
- Webster R, Oliver MA (2007) *Geostatistics for environmental scientists, statistics in practice series*. John Wiley & Son Ltd., New York, p 315
- Yilmaz KK, Hogue TS, Hsu KL, Sorooshian S, Gupta HV, Wagener T (2005) Intercomparison of rain gauge, radar, and satellite-based precipitation estimates with emphasis on hydrologic forecasting. *J Hydrometeorol* 6:497–517
- Zeweldi DA, Gebremichael M, Downer CW (2011) On CMORPH rainfall for stream flow simulation in a small, hortonian watershed. *J Hydrometeorol* 12:456–466